Mon. Not. R. Astron. Soc. **310**, 851–862 (1999)

Spatial wavelet analysis of line-profile variations

R. H. D. Townsend★

Department of Physics and Astronomy, University College London, Gower Street, London WC1E 6BT

Accepted 1999 July 21. Received 1999 May 28; in original form August 29

ABSTRACT

The technique of wavelet analysis is discussed in the context of line-profile variations in rapidly rotating stars undergoing non-radial pulsation. This technique may be used to determine the harmonic degree l of the pulsation using isolated residual spectra; it is able to handle spectra with relatively low signal-to-noise ratio levels, and is well suited to extracting previously unobtainable information from low-quality, patchy data. A demonstration of the technique is presented using data generated from a spectral synthesis code.

Key words: line: profiles – methods: data analysis – stars: early-type – stars: oscillations.

1 INTRODUCTION

High-resolution, high signal-to-noise ratio (S/N) spectroscopic observations of early-type (OB) stars over the past two decades have shown that many such stars exhibit subtle, periodic temporal variations in their absorption-line spectra. Smith & Karp (1976) first reported such line-profile variations (lpv) in sharp-lined (slowly rotating) OB stars; they suggested that these lpv were caused by photospheric velocity fields resulting from non-radial pulsation (NRP), a hypothesis that Osaki (1971) had already used to model variability in β Cephei stars with some success. Smith (1977) subsequently supported this NRP hypothesis with observations and modelling of 53 Per and other slowly rotating OB stars, whilst Walker, Yang & Fahlman (1979) presented similar evidence for lpv in the rapidly rotating, Doppler-broadened O star ζ Oph.

Vogt & Penrod (1983) suggested that the variability in ζ Oph, consisting of characteristic 'bumps' and 'dips' of pseudo-emission and absorption moving across absorption-line profiles, could also be attributed to NRP. More recent observations (Kambe, Ando & Hirata 1990; Reid et al. 1993) of this and other rapidly rotating OB stars (e.g. ϵ Per, Gies & Kullavanijaya 1988; μ Cen, Baade 1988; HD 93521, Howarth & Reid 1993; ζ Pup, Reid & Howarth 1996) has shown that such lpv seem to be commonplace; theoretical studies of NRP in OB stars (Gautschy & Saio 1993; Dziembowski & Pamyatnykh 1993; Kiriakidis, Fricke & Glatzel 1993) suggest that pulsational instability is to be expected in most, if not all, such stars. This is indeed fortuitous, for the existence of NRP in these stars opens them up for scrutiny by the newly emergent field of asteroseismology, which may be able to offer fundamental insights into the interior stellar structures inaccessible to other fields of stellar astrophysics.

It is thus of paramount importance that as much information pertaining to the pulsating star as is available is extracted from spectra exhibiting lpv, so that the data used for asteroseismological studies are of the highest quality. This information can be divided for purposes of discussion into temporal and spatial parts, the temporal relating to the time-dependent behaviour of the lpv, and the spatial relating to the spectral morphology of the lpv at each epoch. Temporal analysis of stellar variability has long been realized using the familiar tool of Fourier analysis, whilst a number of techniques have recently been developed to extract information about the spatial structure of the lpv.

This structure is of interest to the observer, because it contains information relating to the angular dependence of the NRP over the surface of the pulsating star. In non-rotating stars, it can be shown (Unno et al. 1989) that the normal modes of pulsation are proportional to the spherical harmonics $Y_l^m(\theta, \phi)$ (Abramowotz & Stegun 1964), labelled by harmonic degree l and azimuthal order m. In rotating stars, these modes are modified by Coriolis and centrifugal forces, but still in general may have values assigned for l and m (Lee & Saio 1990; Townsend 1997a); it is an aim of lpv analysis to extract these quantities from the spatial structure of the variations. For 53 Per (slowly rotating) stars, this can be achieved using moments methods (Balona 1986; Aerts, De Pauw & Waelkens 1992; Aerts 1996), whilst wavelength-dependent Fourier analysis techniques appear to be more effective for the ζ Oph (rapidly rotating) pulsators (Baade 1988; Gies & Kullavanijaya 1988; Telting & Schrijvers 1997), which show the characteristic redward-migrating bumps and dips in their lpv.

A new method of performing lpv spatial analysis is presented herein, based on the wavelet transform, which is well suited to extracting spatial information from line-profile variable spectra. The following section reviews the underlying methods of lpv spatial analysis, providing a brief overview of Fourier transform based techniques, whilst the subsequent section introduces the wavelet transform. Sections 4 and 5 present some examples of the application of wavelet analysis to lpv, and Section 6 illustrates how the analysis can be used to recover pulsation parameters.

★ E-mail: rhdt@star.ucl.ac.uk

Future work is discussed in Section 7, and the research presented herein is summarized in Section 8.

2 SPATIAL ANALYSIS

In the spatial analysis of lpv, the data that are of principal interest are not the morphology of spectral lines as a whole (although the moments method previously mentioned can readily extract this information), but rather the morphology of the *residual spectra*. These residual spectra can be typically defined as the difference between a given spectrum and some suitably chosen reference spectrum, and provide a measure of the time-dependent departure of a given spectrum from the reference spectrum. A popular choice for the reference spectrum is the mean of all spectra in the data set (e.g. Telting & Schrijvers 1997), which is assumed to provide a close approximation to the underlying time-independent spectrum that would be observed if the star were not variable. However, such a choice is not the only one available, as will be demonstrated in Section 4.

One of the most popular Fourier transform (FT) techniques was pioneered by Baade (1988) and Gies & Kullavanijaya (1988), hereinafter GK88, and subsequently adopted by a number of other authors (e.g. Kambe et al. 1990; Telting & Schrijvers 1997). This technique proceeds by taking the temporal FT of spectra along each wavelength bin, and subsequently, for each temporal period detected, decomposing the time dependence of the residual spectra into sinusoidal signals with periods that are integral submultiples (harmonics) of the fundamental period. The reference spectrum is, formally, the mean spectrum, although this mean is implicit in the method and not actually required for the analysis (indeed, the analysis can be used to actually calculate the mean spectrum). The phase $\Phi(\lambda)$ of the resulting sinusoids at some reference epoch is used as a measure of the spatial morphology of the bumps and dips of pseudo-emission and absorption across line profiles. GK88 suggested that the rate of change of $\Phi(\lambda)$ with respect to wavelength λ at the line centre was a direct measure of the azimuthal order m, resulting from the exp (i$m\phi$) angular dependence of pulsation normal modes; however, Schrijvers et al. (1996) have claimed more recently that $\Delta\Phi$, a related quantity giving the maximum change in $\Phi(\lambda)$ across the line profile, is actually a measure of the harmonic degree l, and it is the change in the phase of the first harmonic that gives information relating to m; strong evidence for this claim has been provided by Telting & Schrijvers (1997), and Howarth et al. (1998) have noted an equivalent relationship between l and the morphology of $\Phi(\lambda)$ with respect to λ.

What is evident is that this rate of change of $\Phi(\lambda)$ across a line profile, which essentially 'counts' the number of bumps and dips in the profile, contains useful information of one form or another about the characteristics of the underlying NRP, and that measuring this rate of change is of fundamental importance. In the following sections, a new method by which this can be achieved is presented; this method can extract spatial information directly from individual residual spectra, in contrast to the GK88-based techniques, which rely on extensive time series to obtain (indirectly) these data.

3 WAVELET ANALYSIS

Wavelet analysis is a technique akin to Fourier analysis, which has the ability to detect periodicities of finite extent in a signal. It has already been used extensively to investigate the temporal structure of photometric variability (Szatmáry, Vinkó & Gál 1994), as it represents the ideal tool with which to study pulsation phenomena such as mode switching and multiple-mode excitations. For a detailed description of the wavelet transform and the discipline of wavelet analysis, the interested reader is referred to Chui (1992) and Szatmáry et al. (1994).

A spatially adapted version of the discrete wavelet transform (DWT) defined by Szatmáry et al. (1994) is used throughout this paper to calculate the wavelet amplitude map (WAM) of a residual spectrum $\mathrm{d}\mathcal{F}(\lambda)$. The WAM, represented herein by $\mathcal{W}(\lambda,\gamma)$, is an absolute function of both spectral wavelength λ and spatial frequency γ; it takes large values at a given (λ,γ) when the spectrum contains a component of approximate spatial period $2\pi/\gamma$ at wavelength λ, and small values otherwise (Szatmáry et al. 1994). The WAM used herein, which is based on the so-called 'Morlet wavelet', is given by the expression

$$\mathcal{W}(\lambda,\gamma) = \sqrt{\gamma}\left|\sum_{j=1}^{N} \mathrm{d}\mathcal{F}(\lambda_j)\exp\left[\frac{\mathrm{i}\gamma(\lambda_j-\lambda)-\gamma^2(\lambda_j-\lambda)^2}{2c'^2}\right]\right|, \quad (1)$$

where λ_j and $\mathrm{d}\mathcal{F}(\lambda_j)$ are the wavelength and spectral flux respectively of the jth wavelength bin of the residual spectrum; it is assumed that the residual spectrum consists of N such bins. It is usually desirable that some of these wavelength bins points are chosen from continuum regions adjacent to the line profile under scrutiny, so that it may be verified that variability in residual spectra is confined to line profiles.

The Morlet wavelet used in the expression for $\mathcal{W}(\lambda,\gamma)$ is essentially a sinusoid modulated by a Gaussian; the parameter c' governs the width of the Gaussian at a given spatial frequency, and is adjusted to alter the trade-off between resolution in spatial frequency and resolution in wavelength (the latter being unrelated to the intrinsic spectral resolution, which is set by the spectrograph itself). Larger c' leads to higher resolution in spatial frequency and lower resolution in wavelength, and vice versa; this trade-off is an inevitable consequence of the localized nature of wavelets, and can be viewed as analogous to the uncertainty principle of quantum mechanics. Throughout this paper, c' was assigned a value of 10, chosen to provide good resolution in spatial frequency and acceptable resolution in wavelength. The finite spatial extent of the residual spectrum does not lead to aliasing problems, because the DWT is a localized transform; furthermore, it provides a two-dimensional (spatial frequency–wavelength) description of the residual spectrum, in contrast to the '$1+1$' dimensions (frequency and phase) of traditional FT analyses (the two-dimensional method of Kennelly, Walker & Merryfield 1992 is discussed in the subsequent section). Note that, because the WAM is an absolute quantity, all phase information is discarded in its evaluation; hence it contains insufficient data to reconstruct the original spectrum, and a fully complex version of the WAM must be retained if an inverse transform is required.

4 APPLICATION TO HEURISTIC LPV

To discuss the application of the DWT to pulsation-originated lpv, it is instructive to use a very simple heuristic model to describe the morphology of the residual spectra. If the bumps and dips of a residual spectrum repeat over a spatial period of $2\pi/\gamma_\mathrm{p}$ and have a temporal frequency of ω, and if the amplitude of the bumps and dips is well described by an envelope function $\mathcal{E}(\lambda)$, then the

residual flux $\mathrm{d}\mathcal{F}(\lambda, t)$ may be written as

$$\mathrm{d}\mathcal{F}(\lambda, t) = \mathcal{E}(\lambda) \exp[\mathrm{i}(\omega t - \gamma_\mathrm{p}\lambda)]. \quad (2)$$

This heuristic model reproduces a set of localized, spatially and temporally, periodic bumps and dips which evolve across the line profile with time, and hence describes at a qualitative level the morphological characteristics of most lpv in rapidly-rotating stars. If equation (2) is substituted into equation (1), the resulting WAM is a function that takes (relatively) large values around a spatial frequency of $\gamma = \gamma_\mathrm{p}$ and over a wavelength range where $\mathcal{E}(\lambda)$ differs significantly from zero, and small values otherwise. To illustrate this, Fig. 1 shows the residual spectrum and associated WAM for lpv calculated using equation 2. The intrinsic spatial frequency γ_p of the lpv was taken to be $1.29\,\mathrm{rad\,\AA^{-1}}$, and a Gaussian was adopted as the envelope function $\mathcal{E}(\lambda)$, with a central height of 0.6 per cent (relative to a rectified continuum level of unity) and a full width at half-maximum equal to that of the He I 6678-Å absorption line modelled in Section 5. These values were used to allow direct comparison between the WAM in Fig. 1 and those in subsequent sections. Plotted over the WAM are curves indicating the peak wavelet amplitude (dotted) and mean (dashed) spatial frequencies at each wavelength; the latter has been calculated using the wavelet amplitude as a weighting function. Both of these curves vary slowly with wavelength, and demonstrate that the WAM is dominated by a wavelet amplitude ridge of approximately constant spatial frequency which extends in wavelength over the variability region. The small degree of wavelength dependence which *is* evident in this ridge is a general

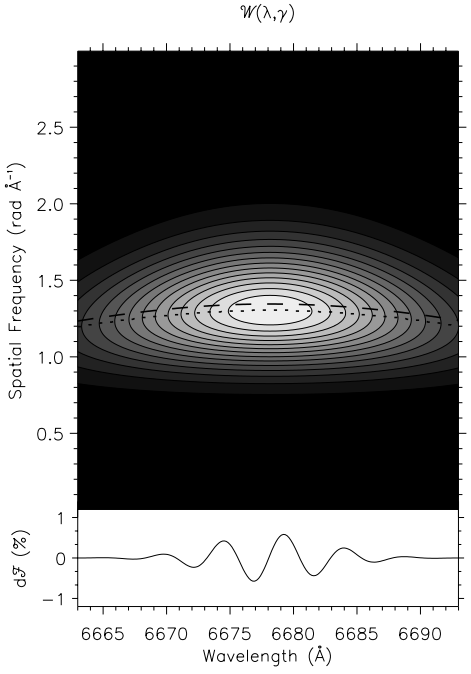

Figure 1. The residual spectrum and associated WAM $\mathcal{W}(\lambda, \gamma)$ for lpv calculated using equation (2), with a Gaussian envelope function $\mathcal{E}(\lambda)$ and a spatial frequency $\gamma_\mathrm{p} = 1.29\,\mathrm{rad\,\AA^{-1}}$. The dotted and dashed lines indicate the position of the peak-amplitude and mean spatial frequencies respectively at each wavelength. The normalization of the WAM is such that black and white correspond to zero and maximum wavelet amplitude respectively, and the contours are drawn at 16 equally spaced intervals between these extrema.

characteristic of WAMs for signals of finite extent, and arises because the approach towards zero of the envelope function $\mathcal{E}(\lambda)$ at the boundaries of the signal effectively lengthens its local period, and thus leads to slightly lower frequencies at these boundaries.

As the spatial phase of the lpv described by $\mathrm{d}\mathcal{F}(\lambda, t)$ at a given epoch may be defined by

$$\Phi(\lambda) \equiv \gamma_\mathrm{p}\lambda, \quad (3)$$

then it is immediately apparent that γ_p is the rate of change of the phase $\Phi(\lambda)$ with respect to λ, discussed in Section 2, and that the WAM may be readily used to measure this rate of change *for a single residual spectrum* when a single pulsation mode dominates the lpv. Of course, this assertion assumes that $\mathrm{d}\mathcal{F}(\lambda, t)$ is a reasonably accurate description of more physically realistic lpv residual spectra. This issue is discussed in the subsequent section, where it is demonstrated that, although the WAMs for such spectra contain more structure than shown in Fig. 1, the results presented in this section still retain a high degree of validity.

There are other points concerning the DWT that recommend its applicability to the study of lpv. Of particular note is that the WAM of equation 2 is time-independent. The reason for this is that the temporal dependence of $\mathrm{d}\mathcal{F}(\lambda, t)$ appears only as a phase term $\exp(\mathrm{i}\omega t)$; since, as was noted previously, phase information is discarded in the calculation of a WAM, it is apparent that this term plays no part in the value of the WAM, and that the WAM is time-independent. This result immediately suggests that the WAMs of more realistic lpv residual spectra will exhibit little time dependence, and that these WAMs may be coadded to improve the S/N of a detection; Sections 5.2 and 5.5 explore these hypotheses. Such coaddition is not constrained by any requirements of complete or extensive time coverage, and may be used to collect all suitable spectra of a pulsating star into one summed 'master-WAM'.

Also worthy of investigation is the result of taking the DWT of the difference between two residual spectra $\mathrm{d}\mathcal{F}_1$ and $\mathrm{d}\mathcal{F}_2$ from epochs t_1 and t_2 respectively. This difference may be written as

$$\begin{aligned}\mathrm{d}\mathcal{F}_1 - \mathrm{d}\mathcal{F}_2 &= \mathcal{E}(\lambda) \exp(\mathrm{i}\gamma_\mathrm{p}\lambda)[\exp(\mathrm{i}\omega t_1) - \exp(\mathrm{i}\omega t_2)] \\ &= \mathcal{E}_{1,2}(\lambda) \exp[\mathrm{i}(\gamma_\mathrm{p}\lambda + \alpha)], \end{aligned} \quad (4)$$

where $\mathcal{E}_{1,2}(\lambda)$ is some modified envelope function (zero if $t_1 = t_2$, and in general dependent on t_1 and t_2) and α is some phase term. The WAMs of this differential and the original residual spectra will not be identical, but they will be *similar* in that they will both exhibit a strong component of spatial frequency γ_p. A similar result exists for the DWT of the sum of two or more spectra, and these results hold even in the case of multiple-mode pulsation. Consequentially, it is of no matter whether the reference spectrum used to prepare residual spectra contains some measure of lpv structure itself – this structure will not affect the results of the wavelet analysis. In fact, a single rectified spectrum from a given epoch may be taken to be the reference spectrum, as long as the other spectra differ sufficiently in temporal phase $\Phi_t \equiv \omega t$ for the modified envelope function $\mathcal{E}_{1,2}(\lambda)$ to have a significantly large amplitude; this powerful feature is demonstrated in Section 5.2. Thus, in principle, wavelet analysis may be performed with as few as two individual spectra.

It is instructive to compare the wavelet analysis technique with the two-dimensional FT method that Kennelly et al. (1992) used to analyse δ Scuti pulsators. They mapped residual spectra of τ Peg

from wavelength into Doppler velocity, and thence, by use of the Doppler imaging approximation, into stellar azimuth ϕ. By taking the two-dimensional (azimuth-time) FT of these transformed spectra, they were able to recover both the pulsation frequency ω and the azimuthal order $|m|$ for four separate pulsation modes of the star. The two-dimensional FT technique is similar to spatial wavelet analysis, in that it calculates the spatial frequencies of the lpv bumps and dips; it hence shares many of the strengths of wavelet analysis. However, although the technique may detect the spatial periodicity of lpv, it cannot reveal the spatial extent of such lpv in the way that spatial wavelet analysis can, because of the non-localized nature of FT sinusoids; this non-localization also leads to spatial aliasing problems.

Note that Kennelly et al. (1992) assumed that all modes detected in τ Peg were sectoral ($l = |m|$) and that the inclination i of the stellar rotation axis to the line-of-sight was close to 90°. The two-dimensional FT technique may be used without these assumptions, but, in light of results presented by Telting & Schrijvers (1997) and in Section 6 of this paper, the spatial frequencies found by Kennelly et al. (1992) should be reinterpreted as a measure of l rather than $|m|$.

5 APPLICATION TO SYNTHETIC LPV

To examine some of the points raised in the preceding section using a more complete physical model of lpv, WAMs were calculated for a number of residual spectra produced by the NRP spectral-synthesis code BRUCE (Townsend 1997a,b), with the inclusion of radial/horizontal velocity fields and temperature/surface-area/surface-normal perturbations. Residual spectra were calculated covering the wavelength range 6663–6693 Å, with a spectral resolution of 0.15 Å; with the exception of Section 5.2, the time-independent mean spectrum was used as the reference spectrum. The spectral region was chosen to span the He I absorption line at 6678 Å, the line originally shown to exhibit variability in ζ Oph (Wallker et al. 1979). The adopted parameters of the model pulsating star are given in Table 1, corresponding approximately to those of ζ Oph (Reid et al. 1993). Unless otherwise indicated, the pulsation amplitude was normalized so that the maximum modulus of the three-dimensional photospheric pulsation velocity was $20\,\mathrm{km\,s^{-1}}$.

5.1 Individual spectra

A single residual spectrum was calculated for an $l = -m = 8$ pulsation mode with a corotating pulsation period of 2 h. This short period corresponds to pressure (p) mode excitation, where the photospheric velocity fields are dominated by radial, as opposed to horizontal, terms. Fig. 2 shows the residual spectrum and associated WAM; a distinct wavelet amplitude ridge, with $\gamma = 1.29\,\mathrm{rad\,Å^{-1}}$ at the line-centre, is evident. The shape and position of this ridge, as shown by the dotted line, are very similar to those shown for the heuristic lpv model in Fig. 1; in contrast, the wavelet-amplitude weighted mean spatial frequency (dashed line) departs significantly from that found for the heuristic model, in particular taking larger values, and thereby indicating the presence of higher spatial frequency components, at the line wings. This departure illustrates the breakdown of the heuristic model, and shows that realistic lpv exhibit a spatial frequency 'chirp' towards the wings; however, this chirp does not appear significantly to distort the ridge, as indicated, and

Table 1. Stellar parameters used to model lpv using the spectral-synthesis code BRUCE.

Quantity	Value
Equatorial rotation velocity $V_{\rm eq}$	$400\,\mathrm{km\,s^{-1}}$
Rotation axis inclination i	60°
Polar temperature $T_{\rm pole}$	38 000 K
Polar radius $R_{\rm pole}$	$9.0\,\mathrm{R_\odot}$
Polar gravity $\log_{10} g_{\rm pole}$	4.0 dex

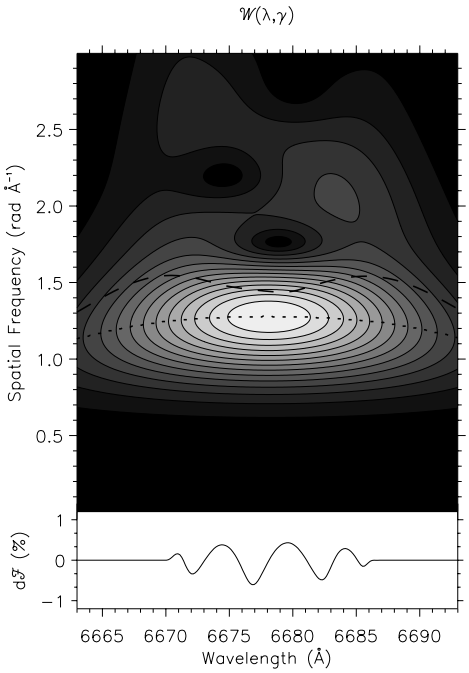

Figure 2. A residual spectrum and associated WAM $\mathcal{W}(\lambda,\gamma)$ for an $l = -m = 8$ pulsation mode. The annotation and normalization of the WAM are the same as in Fig. 1.

therefore it is useful to introduce the concept of the 'principal' spatial frequency for realistic lpv, which corresponds to the intrinsic spatial frequency $\gamma_{\rm p}$ of the heuristic model described by equation (2).

The rate of change of $\Phi(\lambda)$, discussed in Section 2, is given by the value of $\gamma_{\rm p}$ measured from the WAM. There are a number of methods by which this principal spatial frequency can be determined; throughout this paper, with the exception of Section 5.5, $\gamma_{\rm p}$ is taken to be the position of the ridge at the line centre, for reasons of simplicity, and thus in this case takes a value of $1.29\,\mathrm{rad\,Å^{-1}}$. An alternative method, which may give better results with real observational data, is to calculate the average wavelet amplitude by summing the WAM in the wavelength direction, and determine the value of $\gamma_{\rm p}$ from the peak of this average; this approach is used in Section 5.5. Whichever method is chosen, it is important that the same method is used in both the analysis and the pulsation-mode parameter calibration (Section 6).

The ability to extract meaningful asteroseismological data from a single residual spectrum means that, with wavelet analysis, the emphasis of observational studies may be expanded from extensive time-series observations of single stars to extensive few-spectra surveys of entire OB stellar populations; even if analysis of the resultant data is unable to achieve an identification

of pulsation parameters, it is still able to detect underlying (and perhaps temporally aperiodic) spatially periodic line-profile variability, providing the motivation for more intensive studies.

5.2 Temporal stability

In this subsection, the time dependence of lpv WAMs is investigated, and the possibility of using spectra other than the mean spectrum as the reference spectrum is demonstrated. A time series of six spectra, uniformly sampling one (observer's frame) pulsation period, was calculated using the parameters given in the preceding subsection. Five residual spectra were then calculated, using the spectrum at zero temporal phase Φ_t as the reference spectrum, and a master-WAM was formed by coadding these individual WAMs.

Fig. 3 illustrates these residual spectra, their associated WAMs, and the master-WAM. The individual WAMs do show some degree of time dependence, especially in their higher spatial frequency components. This leads to a time dependence in the position of the mean spatial frequency (dashed line), and arises from the departure of realistic lpv from the heuristic model presented in Section 4. However, the wavelet amplitude ridge (dotted line) *is* almost time-independent, and, therefore, so also is the principal spatial frequency $\gamma_{\rm p}$ discussed in the preceding

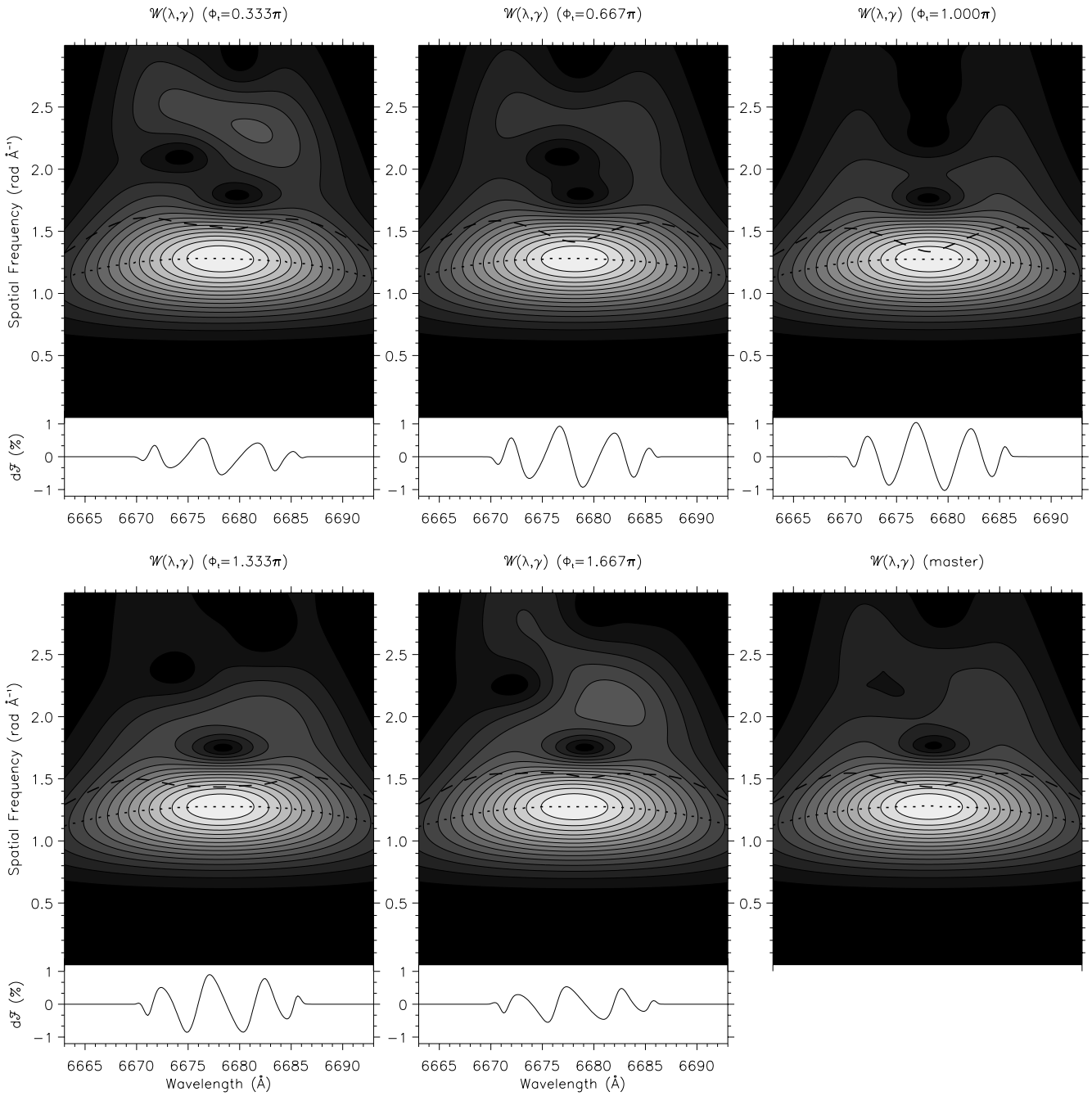

Figure 3. The residual spectra, associated WAMs and master-WAM $\mathcal{W}(\lambda,\gamma)$ for a six-spectrum time series of an $l = -m = 8$ pulsation mode; the spectrum at zero temporal phase Φ_t has been used as the reference spectrum, and is not shown. The annotation and normalization of each WAM are the same as in Fig. 1.

subsection. This result lends support to the validity of forming a master-WAM by coadding residual spectra, discussed in Section 4.

The spatial asymmetry observed in the master-WAM arises from the fact that a single spectrum was used as the reference spectrum, rather than the time-averaged mean spectrum. This choice of reference spectrum also accounts for the observed time dependence of the envelope function $\mathcal{E}_{1,2}$; this envelope function is identically zero at $\Phi_t = 0$ (which is why the spectrum and WAM are not shown at that temporal phase), and at a maximum at $\Phi_t = \pi$.

5.3 Multiple modes

Many early-type stars that exhibit lpv are known to possess more than one temporal period (e.g. ζ Oph, HD 93521). This multiple periodicity can be attributed to the excitation of more than one NRP mode in the star. Since lpv resulting from photospheric velocity fields arise from a perturbation of isovelocity contours on the stellar disc (Townsend 1997b), the formation of such lpv is not an additive process, and the principle of superposition cannot be used to decompose variability resulting from multiple-mode pulsation into separate signals corresponding to each mode excited. Instead, the residual spectrum at a given epoch will be a combination of independent contributions from each pulsation mode, and some time-dependent spatial signals arising from interference between these contributions. This leads to an appreciable degree of time dependence in the WAMs of multiple-mode lpv, and the results presented in the preceding subsection do not apply. However, if the temporal coverage of observations is suitably extended, it is still useful to form a master-WAM for multiple-mode lpv, as the time-dependent interference signals mentioned above will be smoothed out when individual WAMs from differing epochs are coadded. What constitutes a 'suitably extended' temporal coverage in this context is not immediately clear, but a prudent choice would appear to be some multiple of the longest temporal beat period in the observations.

To demonstrate the utility of forming master-WAMs in the case of multiple-mode lpv, and to investigate how well the DWT is able to resolve the spatial structure of each mode, three time series of 96 spectra were calculated using the parameters given in Section 5.1, but with the (multiple excitation of) $l = (2, 8)$, $l = (4, 8)$ and $l = (6, 8)$ modes respectively. In all cases, the azimuthal order m was taken to be -2; it was decided to hold m constant and vary l because, as is demonstrated in Section 6, the WAM of a given pulsation mode is mainly dependent on l, and almost independent of m. The corotating pulsation periods of the $l = 2, 4, 6$ modes were taken to be 8, 4 and 2.667 h respectively; these values were chosen by scaling the 2-h period of the $l = 8$ mode by a factor of $l/8$. Such a scaling corresponds to adopting the asymptotic approximation for p modes (Tassoul 1980) and assuming that all modes exhibit the same number of radial nodes in the Lagrangian displacement. The extent of each time series was taken to be four times the beat period of the appropriate two modes, in the observer's frame. To ensure that each pulsation mode generated approximately equal amplitudes of variability, the velocity amplitudes were taken to be $20\,\mathrm{km\,s^{-1}}$ for the $l = 2, 4, 6$ modes and $40\,\mathrm{km\,s^{-1}}$ for the $l = 8$ mode. Fig. 4 illustrates the master-WAMs corresponding to each of the three time series.

It is apparent that the DWT does pick up the spatial characteristics of the individual modes – this is most evident in the $l = (2, 8)$ panel, where two distinct wavelet-amplitude ridges, corresponding to the $l = 2$ (low-spatial frequency) and $l = 8$ (high-spatial frequency) modes, are well resolved. In the other panels, this resolution is lost as the two ridges merge, although it is still possible to ascertain from $l = (4, 8)$ master-WAM that more than one mode is excited in the star. In cases such as these, it would be prudent to supplement the DWT spatial analysis with a suitable (e.g. FT-based) temporal analysis, which can distinguish multiple modes more easily because of their differing temporal periods.

The merger of ridges for multiple modes with similar l represents one of the weaknesses of the wavelet analysis technique – although the DWT is able to give information concerning both spatial frequency and wavelength, the trade-off between these two variables (Section 3) means that the resolution in spatial frequency can only be increased (by increasing the parameter c' in equation 1) at the expense of the resolution in wavelength, which is not always desirable. The principal way to overcome these resolution problems is to modify the method used to calculate the DWT; this is discussed in Section 7. Another difficulty with the detection of multiple modes using the DWT is the possibility of confusing multiple modes with a single long-period mode; this is discussed in the following subsection.

5.4 Long-period modes

The pulsation parameter K is given by $GM/(\omega_c^2 R^3)$, where ω_c is the pulsation angular frequency in the corotating frame. When K exceeds unity, the photospheric velocity fields become dominated by horizontal components. As these horizontal components only have appreciable projected values towards the stellar limb, pulsation modes with large K, corresponding to gravity (g) modes, will exhibit lpv predominantly at the line wings. This lpv morphology, although encompassed by equation 2, introduces some subtle aspects into the wavelet analysis. To demonstrate this, the residual spectrum discussed in Section 5.1 was recalculated using a corotating pulsation period of 20 h, which leads to a value of 2.07 for K. The residual spectrum, along with the associated WAM, is illustrated in Fig. 5. It is apparent from scrutiny of this figure that the original wavelet amplitude ridge of Fig. 2 has been split in the spatial frequency direction into two distinct ridges, which are shown by the dotted lines.

Schrijvers et al. (1996) have noted that modes with large K lead to lpv that exhibit a discontinuity in $\Phi(\lambda)$ of π radians near the line centre; this phase jump leads to difficulties in their analysis, and is responsible for the frequency splitting observed in Fig. 5 (see also fig. 13b of Szatmáry et al. 1994). The explanation for this is that the jump introduces a degree of spatial periodicity in the envelope function $\mathcal{E}(\lambda)$ appearing in equation 2, which corresponds to a periodic amplitude modulation of the lpv. Such modulation can be considered as the result of beating between two spatial frequencies γ_1 and γ_2, which obey the relations

$$\gamma_1 = \gamma_p + \gamma_e \tag{5}$$

and

$$\gamma_2 = \gamma_p - \gamma_e, \tag{6}$$

where γ_e is the spatial beat frequency corresponding to the periodicity in $\mathcal{E}(\lambda)$. When the WAM is calculated, the DWT will pick up these two spatial frequencies, leading to the two ridges observed in Fig. 5; it is evident that the spatial frequency γ_p of the lpv themselves is given by $(\gamma_1 + \gamma_2)/2$, while that of the envelope

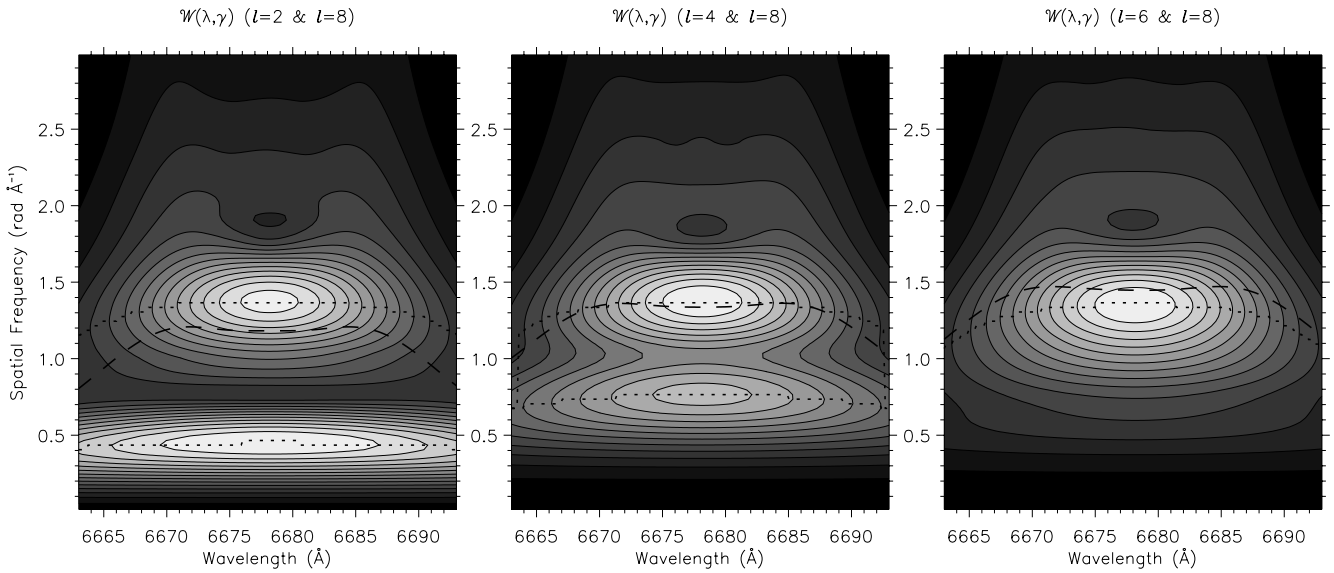

Figure 4. The master-WAMs $\mathcal{W}(\lambda,\gamma)$ for 96-spectra time series of $l = (2, 8)$, $l = (4, 8)$ and $l = (6, 8)$ multiple pulsation modes. In all cases, the azimuthal degree m was -2. The annotation and normalization of each master-WAM are the same as in Fig. 1.

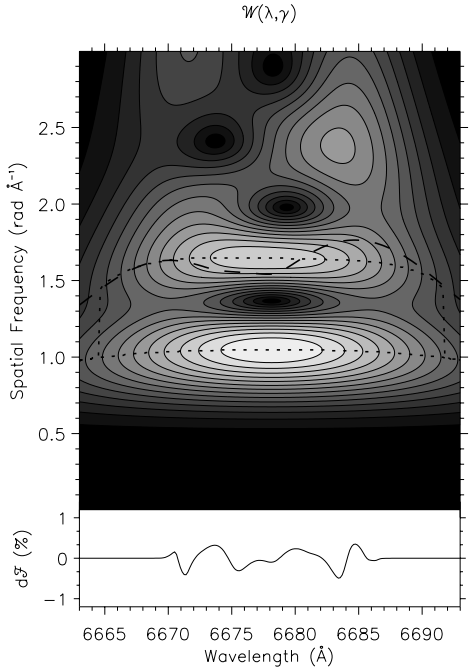

Figure 5. A residual spectrum and associated WAM $\mathcal{W}(\lambda,\gamma)$ for a long-period $l = -m = 8$ pulsation mode. The annotation and normalization of the WAM are the same as in Fig. 1.

function will be given by $(\gamma_1 - \gamma_2)/2$. Therefore, it remains possible to recover γ_p from a WAM in the case of lpv caused by a long-period pulsation mode.

It may be argued that the WAM in Fig. 5 could also result from a residual spectrum exhibiting lpv because of two pulsation modes, as was demonstrated in the preceding subsection (see also Fig. 4). To distinguish between these cases, some technique other that wavelet analysis must be used, either to ascertain whether multiple modes are present in the star, or to calculate a value for K. Evaluating the correct value of K is non-trivial – it requires knowledge of the corotating frequency ω_c, which in turn depends on the azimuthal order m and the rotation angular frequency Ω. Estimates of K may also be obtained by considering the excitation mechanism thought to generate pulsation in the star under observation, because knowledge of this mechanism indicates whether p modes (small K) or g modes (large K) are expected to be prevalent.

5.5 Effects of noise

Of great interest to the observer is how the wavelet analysis technique is affected by noise, because lpv in pulsating stars are typically observed with amplitudes of the order of the spectral noise level. The effect of noise is to add a contaminatory background signal to residual spectra; this background signal will lead to spurious features in the corresponding WAMs, distorting and possibly obscuring any wavelet amplitude ridges corresponding to lpv. To demonstrate this phenomenon, synthetic noise drawn from a Gaussian distribution with a standard deviation Δ was added to each wavelength bin of the residual spectrum presented in Section 5.1, and the resulting WAM was calculated. Fig. 6 illustrates the noisy residual spectra and corresponding WAMs for Δ values of 0.002, 0.004, 0.010, 0.020, 0.040 and 0.100; these values correspond to S/N levels of 500, 250, 100, 50, 25 and 10 respectively, because the S/N is given by $1/\Delta$ for a continuum flux of unity.

In this figure, the ridge corresponding to the principal spatial frequency of the lpv is evident in the WAMs for S/N levels of 500, 250 and 100, although in the latter case the ridge cannot be considered to be a reliable detection, as there are other, stronger, ridges and peaks introduced by the noise. At lower S/N levels, the ridge has been swamped by the noise and is no longer visible. This is to be expected, because the peak semi-amplitude of the lpv is approximately 0.6 per cent of the continuum in this case, and therefore the lpv signal is dominated by the noise signal for a S/N below approximately 166.

However, it is possible to recover the ridge by using a master-WAM in the analysis, rather than the WAM of an individual spectrum. To demonstrate this, a time series of 24 spectra, covering one pulsation period, was generated with the addition of

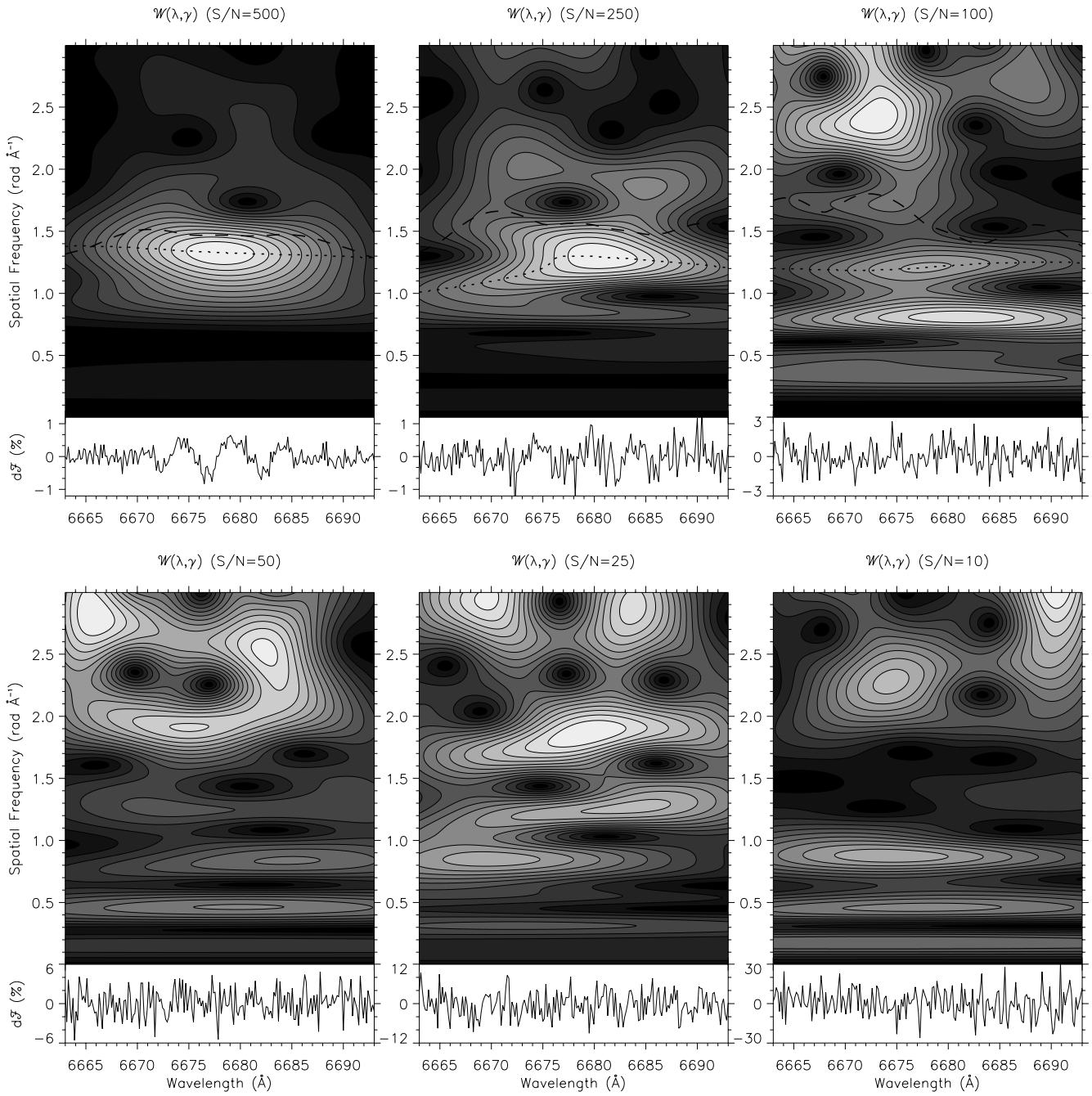

Figure 6. The residual spectra and associated WAMs $\mathcal{W}(\lambda,\gamma)$ for an $l = -m = 8$ pulsation mode, with S/N levels of 500, 250, 100, 50, 25 and 10. The annotation and normalization of each WAM are the same as in Fig. 1.

noise at a S/N level of 50, using the same pulsation parameters as those in Section 5.1. WAMs for each of these spectra were coadded to form a master-WAM, illustrated in Fig. 7. The ridge corresponding to the lpv, with a peak spatial frequency of $\gamma \approx 1.3\,\mathrm{rad\,Å^{-1}}$, has apparently been recovered, although the 'contrast' between this ridge and surrounding regions of the master-WAM is much lower than that in Fig. 2, and it is not immediately clear what confidence level can be assigned to the detection. This reduced contrast results from the fact that wavelength amplitude can only take positive values (see equation 1), and therefore noise signals in one spectrum do not cancel those in another spectrum when the master-WAM is calculated – the noise produces a background bias at each spatial frequency and wavelength in the master-WAM, which scales linearly with the reciprocal of the S/N.

To investigate this issue further, and to place the noise characteristics of wavelet analysis on a more quantitative footing, 35 000 WAMs were calculated, each based on a residual spectrum covering the wavelength range 6663–6693 Å with a spectral resolution of 0.15 Å and consisting solely of noise at a S/N level of 50. Of these original WAMs, 10 000 were used to calculate a set of 5000 two-spectra master-WAMs, and a further 20 000 were used to calculate a set of 5000 four-spectra master-WAMs, leaving a remaining set of 5000 individual (single-spectrum) WAMs. Subsequently, for each WAM in each of these three sets, the average wavelet amplitude per wavelength bin was calculated by

summing the WAMs in the wavelength direction and then dividing by the number of bins. Finally, for each resulting set of 5000 average wavelet amplitude curves, the mean and standard deviation σ were determined as functions of spatial frequency.

Fig. 8 illustrates these mean curves normalized by N_s, where N_s is the number of spectra used to calculate each WAM in the corresponding set; the normalized curves, which are observed to be independent of N_s, indicate the background bias per wavelength bin per spectrum in master-WAMs caused by noise. Also shown in the figure is the mean plus and minus the standard deviation σ, again normalized by N_s; these curves indicate the 1σ range of statistical fluctuations on the bias. This range scales as $1/\sqrt{N_s}$, so, as more spectra are used to calculate the master-WAM, the statistical fluctuations on the background bias decrease.

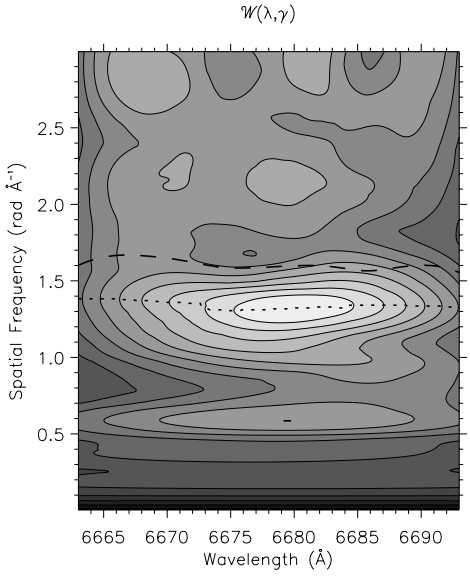

Figure 7. The master-WAM $\mathcal{W}(\lambda,\gamma)$ for a 24-spectrum time series of an $l = -m = 8$ pulsation mode, with a S/N level of 50. The annotation and normalization of the master-WAM are the same as in Fig. 1.

This last point is the reason why master-WAMs are able to recover features caused by lpv from individual WAMs which have been swamped by noise; as N_s is increased, it becomes more and more probable that an observed deviation from the background bias is not attributable to the random nature of the noise. To demonstrate this, Fig. 9 shows the average wavelet amplitude per wavelength bin per spectrum for the 24-spectrum master-WAM illustrated in Fig. 7, calculated using the method described previously. Also shown is the background bias resulting from noise, and the 1- and 2σ range of statistical fluctuations for this bias, for $N_s = 24$ and a S/N level of 50. From inspection of this figure, it is evident that only one wavelet amplitude peak falls outside the 2σ range, deviating from the background bias by somewhat more than 4σ; if the Gaussian nature of the noise is unaffected by the DWT procedure, then probability of this peak being a noise artefact is of the order of 1 part in 10^5, and the apparent recovery of the ridge shown in Fig. 7 is confirmed at a high confidence level. However, such confidence levels must be quoted with caution, because the assumption of the manner in which noise propagates through the DWT may not be valid. Furthermore, rectification errors in the calculation of residual spectra, which are likely at the low S/N levels discussed herein, may generate artificial structure in the lpv, which in turn may lead to spurious detections that appear to have high confidence levels attached to them (although one would expect such errors to lead solely to low-frequency features in the resulting WAMs). These issues, and more generally the noise characteristics discussed herein, certainly merit further research (see Section 7).

On a final note, it is evident that the spatial frequency γ_p of the peak in Fig. 9 is somewhat higher than the value found in Section 5.1; the reason for this is that, even though the peak is caused by lpv rather than noise, the noise still distorts its shape and position somewhat. This distortion can be minimized both by increasing N_s

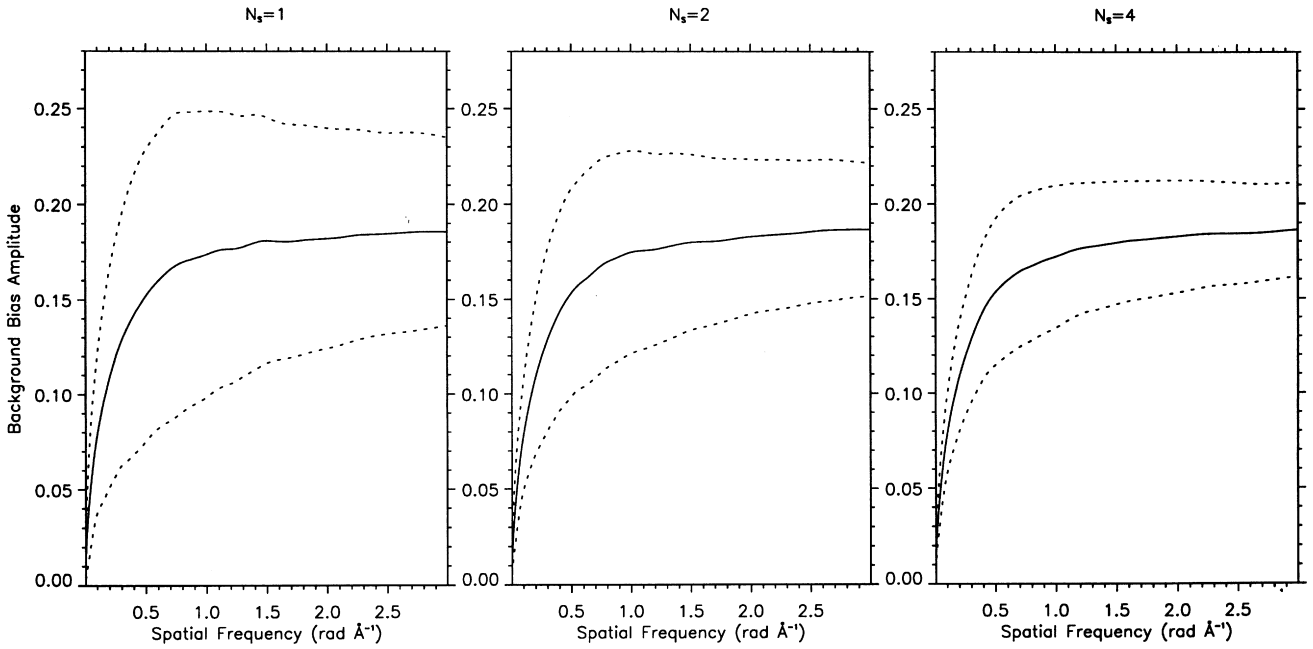

Figure 8. The background bias per wavelength bin per spectrum (solid) caused by noise for master-WAMs calculated using $N_s = 1$, 2 and 4 spectra, with a S/N level of 50. The dotted lines show the 1σ limits on this bias.

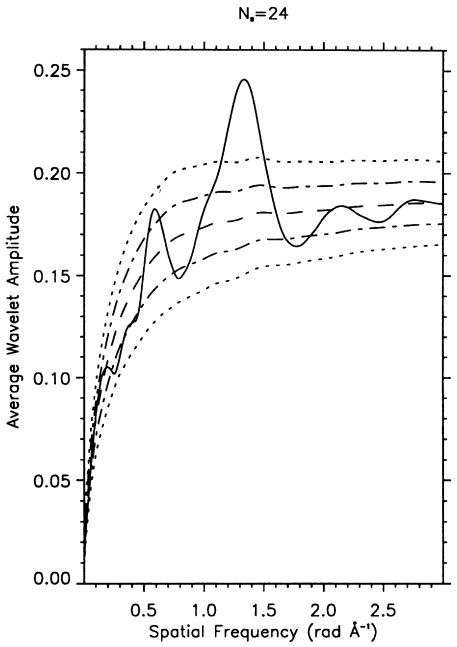

Figure 9. The average wavelet amplitude per wavelength bin per spectrum (solid line) for the 24-spectrum master-WAM shown in Fig. 7. Also shown is the background bias caused by noise (dashed line), and the 1- and 2σ limits on this bias (dot–dashed and dotted lines, respectively). The S/N level adopted for the calculations was 50.

and deducting the background bias from the average wavelet amplitude when the position of the peak is to be determined.

6 EXTRACTING PULSATION PARAMETERS

As was demonstrated in the previous section, wavelet analysis represents an powerful tool with which to determine the principal spatial frequency γ_p of the bumps and dips appearing in lpv. However, some method of mapping the value of γ_p into mode parameters l and m is required for this technique to be quantitatively useful. To determine this mapping, three sets of residual spectra time series, corresponding to stellar inclinations i of 30°, 60°, and 85° respectively, were calculated using the procedure outlined in Section 5. Each set contained 256 time series of 24 residual spectra, uniformly sampling pulsation period, with l and m extending over $0 \leqslant l \leqslant 15$ and $-l \leqslant m \leqslant l$. Master-WAMs were calculated for these time series, and the value of γ_p, the principal spatial frequency, was determined for each (l, m) pair in each set using the method described in Section 5.1. Fig. 10 illustrates these values, scaled by $\sin(i)$, as a function of l and m, for each value of i indicated; this scaling is to take into account the different rotationally broadened linewidths at different inclinations, because the principal spatial frequency will vary as the reciprocal of the line width for a given number of lpv bumps and dips in the line profile.

For inclinations of 30° and 60°, this figure shows that, whilst γ_p depends only weakly on m, it exhibits a strong, near-linear dependence on the harmonic degree l; this concurs with the relationship between l and $\Delta\Phi$ demonstrated by Telting & Schrijvers (1997). At an inclination of 85°, the dependence on l appears to break down for modes with an odd value of $l - |m|$, in that the value of γ_p is significantly larger than that 'expected'. A similar phenomenon has been reported by Schrijvers et al. (1996), who found that such modes exhibit a doubling in the number of lpv bumps and dips at inclinations near 90°; this behaviour arises because the pulsation of such modes is nearly anti-symmetrical with respect to the equatorial plane at inclinations close to equator-on, and lpv at the principal spatial frequency are almost completely suppressed because of cancellation effects between the two hemispheres, leaving only components of higher spatial frequencies.

Telting & Schrijvers (1997) used Monte Carlo simulations to derive an empirical formula relating l to $\Delta\Phi$. In their simulations, they varied a number of parameters in addition to l and m, to investigate the dependence of $\Delta\Phi$ on other quantities, and therefore their formula can be applied to a wide variety of pulsation-originated lpv. A corresponding formula, relating l to γ_p, is not derived herein, as only the inclination has been varied in this work; furthermore, such a derivation would discard possibly important information concerning the dependence of γ on m at intermediate inclinations.

7 FUTURE WORK

This paper serves to introduce the possibility of using the DWT to probe lpv spatial structure, and is not meant to be exhaustive. There are a number of investigations and improvements that need to be performed before this new technique can fulfil its true potential. Above all, the DWT must be used with caution, for, as Szatmáry et al. (1994) stress, it is no 'magic box' by which all lpv analysis problems can be solved. Difficulties distinguishing between large-K and multiple-mode pulsation – and indeed resolving multiple modes − have already been pointed out (Section 5.4); other situations where unwary use of wavelet analysis leads to misidentifications may exist, awaiting discovery. On a more general note, spatial wavelet analysis provides *no* temporal information about lpv, and cannot replace the use of the FT for temporal analysis.

An area certainly worthy of attention in the development the technique is the search for the most appropriate wavelet to use in calculating the DWT of residual spectra. The use of such an optimal wavelet will presumably make wavelet amplitude ridges sharper and more localized in spatial frequency, leading to greater accuracy in the determination of γ_p, and also higher resolution in frequency for the separation of multiple modes. The expression for $\mathcal{W}(\lambda,\gamma)$ given by equation (1) uses the Morlet wavelet, a sinusoid modulated by a Gaussian. Whilst this corresponds in the crudest sense to the form of small-K lpv themselves (as can be seen by comparing Fig. 1 and Fig. 2), a search must be made for the aforementioned optimal wavelet (if it exists), so as to increase the resolution and accuracy to which γ_p is known. This increased resolution will be of most importance in analysing the spectra of stars pulsating in multiple modes, because the master-WAMs of such spectra exhibit multiple ridges (Section 5.3), which must be well separated for clear mode identifications to be made.

One modification to the DWT wavelet that immediately suggests itself is the introduction of a chirp at the line wings. Such a chirp appears in the lpv themselves (Section 5.1), because of the dependence of the projected rotation velocity on the sine of the azimuth ϕ, rather than on ϕ itself. The wavelength−azimuth mapping used by Kennelly et al. (1992) could be used to implicitly introduce the chirp into the DWT wavelet by performing

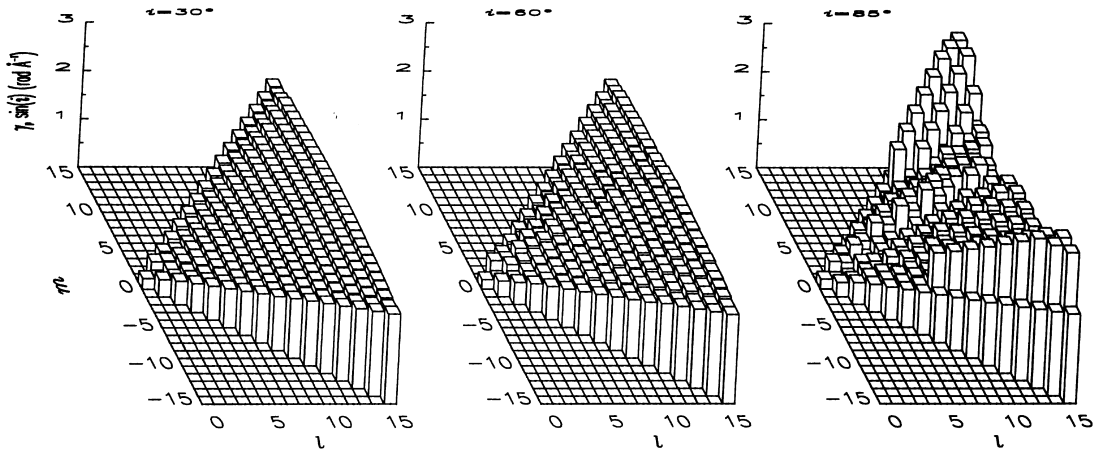

Figure 10. The principal wavelet spatial frequency γ_p, scaled by sin i, as a function of harmonic degree l and azimuthal order m, for inclinations i of 30°, 60° and 85°.

calculations in azimuth space rather than wavelength space; presumably, the higher-frequency features present in the line wings of Figs 2, 3 and 5 would be reduced in amplitude, resulting in a 'cleaner' WAM. It is anticipated that this modification to the method will be investigated in a future paper.

Another important issue under consideration for future investigation is the dependence of γ_p on parameters other than l, m and i. This will allow wavelet analysis to be used with confidence in situations where these other parameters (such as pulsation period, degree of non-adiabacity, etc.) are not known a priori, and thus increase the generality of the discussion. Furthermore, it would be interesting to discover whether the DWT can extract not only l (as was shown in Section 6), but also m, from residual spectra, as the FT analysis of Telting & Schrijvers (1997) is able to do. Other areas also under consideration are a more extensive examination of the noise characteristics of the DWT, building on the results presented in Section 5.5, and an examination of the effect of line blends on spatial wavelet analysis; such blends may exhibit lpv with a phase jump around the blending region, which could lead to the spatial frequency spitting demonstrated in Section 5.4.

8 SUMMARY

The technique of spatial wavelet analysis has been used to analyse spectra exhibiting pulsation-originated lpv and extract information concerning the harmonic degree l of the underlying pulsation. This technique can be applied directly to as few or as many individual spectra as are available, with no reference to the time coverage or completeness of the spectra required, in contrast to Fourier analysis techniques (Baade 1988; Gies & Kullavanijaya 1988; Telting & Schrijvers 1997), which generally require extensive time-series spectra to achieve (indirect) spatial analyses (although they *do* provide accompanying temporal information, which the wavelet analysis technique does not). Variability resulting from both p-mode (small-K) and g-mode (large-K) pulsation has been analysed using the technique, as has that resulting from multiple-mode pulsation. The noise characteristics of spatial wavelet analysis have also been investigated, and it has been demonstrated that the use of master-WAMs can be used to extend the analysis down to low S/N levels.

Although the technique has been used herein to determine the value of l for the pulsation mode generating the lpv, spatial wavelet analysis may be used to detect any form of spatially periodic variability in spectra, and is not just tied to the analysis of pulsation-originated lpv. Whatever the ultimate field of study, however, it is hoped that spatial wavelet analysis will prove to be a useful new tool with which to study line-profile variability, especially in low-quality data; a future paper is therefore planned to develop this tool.

ACKNOWLEDGMENTS

I thank Ian Howarth for both his support for and input to the research behind this paper, and Andy Reid for his helpful comments. I also thank the anonymous referee, who provided many useful suggestions on how the paper could be improved. This work has been supported by the Particle Physics and Astronomy Research Council of the United Kingdom.

REFERENCES

Abramowitz M., Stegun I., 1964, Handbook of Mathematical Functions, Appl. Math. Ser. 55, National Bureau of Standards, USA
Aerts C., 1996, A&A, 314, 115
Aerts C., De Pauw M., Waelkens C., 1992, A&A, 266, 294
Baade D., 1988, in Cayrel de Strobel G., Spite M., eds, IAU Symp. 132, The Impact of Very High S/N Spectroscopy on Stellar Physics. Kluwer, Dordrecht, p. 217
Balona L. A., 1986, MNRAS, 219, 111
Chui C. K., 1992, Wavelets: A turotial in Theory and Applications, Academic Press, Boston
Dziembowski W. A., Pamyatnykh A. A., 1993, MNRAS, 262, 204
Gautschy A., Saio H., 1993, MNRAS, 262, 213
Gies D. R., 1996, in Strassmeier K. G., Linsky J. L., eds, Stellar Surface Structure, IAU, Netherlands, p. 121
Gies D. R., Kullavanijaya A., 1988, ApJ, 326, 813
Howarth I. D., Reid A. H. N., 1993, A&A, 279, 148
Howarth I. D., Townsend R. H. D., Clayton M. J., Fullerton A. W., Gies D. R., Massa D., Prinja R. K., Reid A. H. N., 1998, MNRAS, 296, 949
Kambe E., Ando H., Hirata R., 1990, PASJ, 42, 687
Kennelly E. J., Walker G. A. H., Merryfield W. J., 1992, ApJ, 400, L71
Kiriakidis M., Fricke K. J., Glatzel W., 1993, MNRAS, 264, 50
Lee U., Saio H., 1990, ApJ, 349, 570
Osaki Y., 1971, PASJ, 23, 485
Reid A. H. N., Howarth I. D., 1996, A&A, 311, 616

Reid A. H. N. et al., 1993, ApJ, 417, 320
Schrijvers C., Telting J. H., Aerts C., Ruymaekers E., Henrichs H. F., 1996, A&AS, 121, 343
Smith M. A., 1977, ApJ, 215, 574
Smith M. A., Karp A. H., 1976 in Cox A. N., Deupree R. G., eds, Proc. Solar and Stellar Pulsation Conf., Los Alamos Publ., USA, p. 289
Szatmáry K., Vinkó J., Gál J., 1994, A&AS, 108, 377
Tassoul M., 1980, ApJS, 43, 469
Telting J. H., Schrijvers C., 1997, A&A, 317, 723
Townsend R. H. D., 1997a, MNRAS, 284, 839
Townsend R. H. D., 1997b, PhD Thesis, University of London,
Unno W., Osaki Y., Ando H., Saio H., Shibahashi H., 1989, Nonradial Oscillations of Stars, University of Tokyo Press, Tokyo
Vogt S. S., Penrod G. D., 1983, ApJ, 275, 661
Walker G. A. H., Yang S., Fahlman G. G., 1979, ApJ, 233, 199

This paper has been typeset from a TEX/LATEX file prepared by the author.